Letter

Electron-capture decay rate of ^{7}Be encapsulated in a C_{70} fullerene cage

Tsutomu Ohtsuki [1,*] Riichi Kuwahara [2,†] and Kaoru Ohno [3,‡]

[1]*Institute for Integrated Radiation and Nuclear Science, Kyoto University, Asashiro-Nishi, Kumatori-cho, Sennan-gun, Osaka 590-0494, Japan*

[2]*Dassault Systèmes K. K., ThinkPark Tower, 2-1-1 Osaki, Shinagawa-ku, Tokyo 141-6020, Japan*

[3]*Department of Physics, Yokohama National University, 79-5 Tokiwadai, Hodogaya-ku, Yokohama 240-8501, Japan*

(Received 14 February 2023; accepted 22 May 2023; published 5 July 2023)

The decay rate of ^{7}Be electron capture in C_{70} and Be metal was measured employing a reference method. The half-life ($T_{1/2}$) of ^{7}Be endohedral C_{70} (^{7}Be@C_{70}) was found to be $T_{1/2} = 52.49 \pm 0.04$ d at room temperature ($T = 293$ K) and $T_{1/2} = 52.42 \pm 0.04$ d at liquid helium temperature ($T = 5$ K). Furthermore, the $T_{1/2}$ of ^{7}Be in Be metal was $T_{1/2} = 53.25 \pm 0.04$ d at room temperature ($T = 293$ K) and $T_{1/2} = 53.39 \pm 0.03$ d at liquid helium temperature ($T = 5$ K). These values for ^{7}Be@C_{70} at $T = 5$ K are approximately 1.6%(1.8%) smaller than those for ^{7}Be in Be metal at $T = 293$ K ($T = 5$ K), indicating the difference in the electron wave functions for ^{7}Be inside C_{70} and ^{7}Be in C_{60} and Be metal. The average charge transfer from the $L(2s)$ electrons of the ^{7}Be atom influences such variations in the decay constant ($\lambda = \ln 2/T_{1/2}$) in the environment. The experimental and theoretical investigations revealed that the change in the EC-decay rate of ^{7}Be could be largely related to the potential configurations and the environment inside C_{60} and/or C_{70} cages. The motion of ^{7}Be inside cages was found to be restricted according to temperature.

DOI: 10.1103/PhysRevC.108.L011301

More than 70 years ago, Segrè, Daudel, Kraushaar *et al.* independently suggested that the decay constant (λ) of certain radioactive nuclides may be altered by varying the electron density [$\rho(0)$] in the vicinity of the nucleus [1–4]. Since then, several groups have experimentally investigated variations in λ (namely, $T_{1/2}$, which is related to λ as $T_{1/2} = \ln 2/\lambda$) in electron capture (EC) and/or internal conversion (IC) under different chemical and physical environments to observe its effects. The most frequently used nuclides for such studies were ^{7}Be (and/or ^{99m}Tc), and summaries of earlier studies on orbital electron capture decay (EC-decay) were provided by Emery [5]. The λ of EC-decay can be proportional to electron density [$\rho(0)$] at the nucleus site a ^{7}Be atom.

Experimentally determining the EC-decay rate of ^{7}Be compounds remains challenging. Several observations of variations in $T_{1/2}$ for different chemical forms [6–9], pressures [8,10–12], and host metals [13–20] have been reported. From earlier data, the $T_{1/2}$ of ^{7}Be as a function of different chemical forms and/or host materials has been limited to approximately 0.2% and more in some cases (even though some reports found a difference of at most 1% [11,14]). Therefore, further precise measurements are still needed to obtain the absolute EC-decay rate under different chemical and/or physical circumstances.

Our previous study reported that several atoms can create substitutional and/or endohedral fullerenes (C_{60} and/or C_{70}). Herein, we realized the formation of endohedral fullerenes via the nuclear recoil of several foreign atoms following nuclear reactions [21–25].

In particular, we measured the $T_{1/2}$ of ^{7}Be when it is encapsulated in a C_{60} cage (^{7}Be@C_{60}) with ^{7}Be in Be metal as a reference. We observed large variations in λ in ^{7}Be inside the C_{60} [26,27]. This implied that the ^{7}Be atoms are in a unique environment inside C_{60} cage. Subsequently, we provided certain theoretical interpretations [27,28]. According to this study, the ^{7}Be atom is the most stable and $\rho(0)$ is the highest at the center of a C_{60}. However, the ^{7}Be atom becomes slightly less stable and $\rho(0)$ decreases by 2% under the five-membered rings. Therefore, the ^{7}Be atom is frozen at the center of C_{60} with a higher EC-decay rate at a controlled low temperature, whereas it undergoes rachet or tumbling motion inside C_{60} with a lower EC-decay rate at a fixed room temperature.

Recently, several studies have further expanded the theoretical estimations of the EC-decay rate of ^{7}Be encapsulated in C_{60} and/or C_{70} [29–32]. Because of the potential configurations and/or dynamical motions of a foreign atom inside C_{60} and C_{70} and the larger size of fullerenes [33–37], the electron contact density [$\rho(0)$] on the ^{7}Be nuclei can be significantly affected by the electron environment of C_{60}, C_{70}, etc. Therefore, comparisons of the $T_{1/2}$ of ^{7}Be inside C_{60} and C_{70} are an intriguing research prospect.

In this study, we demonstrate the change in the EC-decay rate of ^{7}Be inside C_{70} at room ($T = 293$ K) and liquid He ($T = 5$ K) temperatures. Furthermore, based on the C_{60} and C_{70} cage dependence for the EC-decay rate, first-principle calculations were performed using DMol^{3} [38,39], which uses

*ohtsuki.tsutomu.d09@kyoto-u.jp
†Riichi.KUWAHARA@3ds.com
‡ohno@ynu.ac.jp

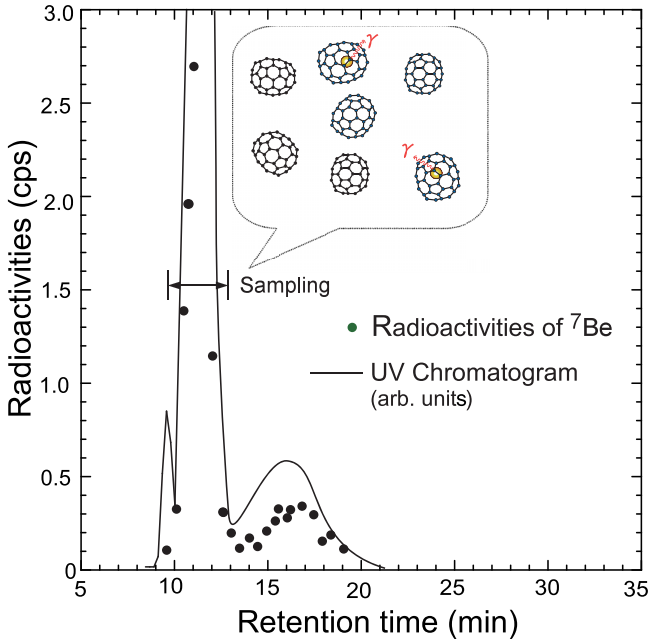

FIG. 1. HPLC elution curves of the soluble portion of the crude extract in the proton-irradiated sample of ^{7}Li and C_{70}. Here, the ^{7}Li$(p,n)^7$Be reaction leads to ^{7}Be production. The vertical axis indicates the 478 keV γ-ray radioactivities (cps) of ^{7}Be in each fraction (solid circles) and absorbance of the UV chromatogram of C_{70} (in arb. unit). The first peak (10–13 min) was collected for the measurement.

numerical localized orbitals. Atom endohedral C_{70} can be produced by inserting foreign atoms into pre-existing C_{70}. The proton-irradiated sample of ^{7}Li with C_{70} results in the production of ^{7}Be. We produced such endohedral C_{70} (^{7}Be@C_{70}) via nuclear recoil implantation [40] (and, e.g., for C_{60} [26]). After irradiation, we performed a high performance liquid chromatography (HPLC) process to separate ^{7}Be@C_{70} with 5 PPB columns. For better understanding, the HPLC elution curves and the ^{7}Be radioactivities of the soluble portion of the crude extracted are shown in Fig. 1. The vertical axis shows the 478 keV γ-ray radioactivities in counts/s (cps) of ^{7}Be in each fraction (solid circles) and the absorbance of the UV-chromatogram of C_{70} (solid curve). The statistical errors of the γ-ray radioactivities (cps) were within the solid circles. To obtain a measurement sample, the solution that corresponded to a C_{70} fraction was evaporated, and finally, the C_{70} sample containing ^{7}Be@C_{70} was converted into a solid tablet by evaporation and press procedures. Subsequently, the endohedral C_{70} (^{7}Be@C_{70}) was confirmed by measurement of the 478 keV γ rays of ^{7}Be.

Herein, we realized the insertion process based on experimental and theoretical studies. An *ab initio* molecular dynamic simulation was performed to demonstrate the feasibility of a direct insertion process. The Be ion easily penetrates the cage through the center of the six-membered ring, and it passes deep into the C_{70} ion and returns to a stable position where it is trapped inside the cage [40]. Other advanced and recent discussions are presented below.

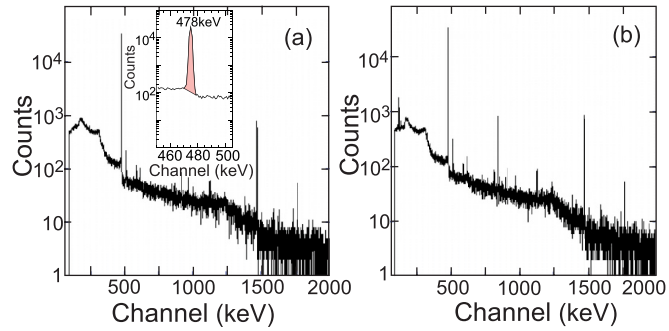

FIG. 2. Typical γ-ray spectra of ^{7}Be for (a) ^{7}Be@C_{70} at $T = 5$ K and (b) ^{7}Be in Be metal at $T = 293$ K. The expanded scale around $E_\gamma = 478$ keV is shown in (a).

For the reference sample, the production of ^{7}Be in Be metal also involved several different procedures. The ^{7}Be isotope was produced in the ^{9}Be$(\gamma, 2n)^7$Be reaction in stable Be metal (tablet with diameter and thickness of 10 and 0.3 mm, respectively) through bremsstrahlung irradiation (with 50 MeV electrons) via an electron linear accelerator (LINAC, Tohoku University), as described in [26]. Subsequently, we used a reference method to measure the $T_{1/2}$ of ^{7}Be in C_{70} (^{7}Be@C_{70}) and that of ^{7}Be in Be metal.

We measured the condition at a fixed room temperature ($T = 293$ K using a high-performance air-conditioner in the measurement) and at He temperature ($T = 5$ K using a cryostat device). To measure the $T_{1/2}$ at $T = 5$ K, the ^{7}Be@C_{70} sample was placed on top of a He closed-cycle cryostat. The two samples, ^{7}Be@C_{70} (fastened in the cryostat) and ^{7}Be in Be metal, were placed in a computer-controlled sample changer that moved the samples precisely in front of a γ-ray (HPGe) detector every 6 h (including 120 s for the sample moving time and the dead time of the measurement system). In the system, the time of the computer's internal clock was exactly and constantly calibrated by a time-standard signal every 10 min distributed via a long-wave radio center in Japan [26,27]. The dead time in the data acquisition system was less than 15 s for each run.

Therefore, uncertainty due to the dead time was less than 0.04%. This arrangement (reference method for each of the two samples) allowed the consistent measurement of the EC-decay rate of the two samples while reducing systematic errors. The 478 keV γ-ray radioactivities emanating from the ^{7}Be were stably measured over 200 consecutive days

Typical two γ-ray spectra obtained for the ^{7}Be@C_{70} at $T = 5$ K and ^{7}Be in Be metal at $T = 293$ K are shown in Figs. 2(a) and 2(b), respectively. The expected line at $E_\gamma = 478$ keV and a natural background line at $E_\gamma = 1461$ keV can be observed as two giant peaks. No peak was observed at $E_\gamma = 478$ keV in the absence of ^{7}Be sources. However, a relatively large peak, ^{54}Mn produced by the (γ, n) reaction from the impurity of ^{55}Mn inside Be metal, was observed in ^{7}Be in Be metal [Fig. 2(b)]. The radioactivities associated with the decay of ^{7}Be ($E_\gamma = 478$ keV) can be uniquely analyzed through the identification of characteristic γ rays. A direct summation method was used to obtain the peak area

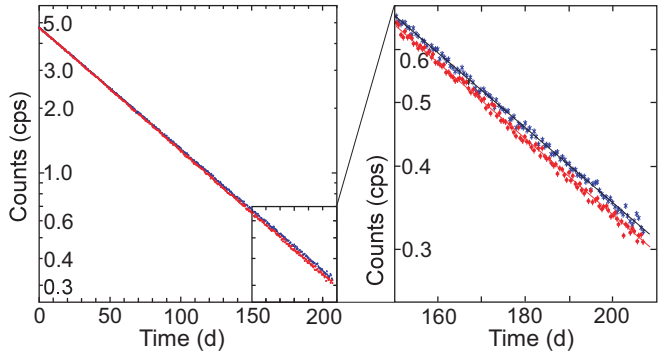

FIG. 3. Exponential decay curves (cps) of ^{7}Be in the samples of ^{7}Be@C_{70} at $T = 5$ K and ^{7}Be in Be metal at $T = 293$ K. The figure on the right corresponds to the decay intervals of 150–210 d and is displayed with an expanded scale.

($E_\gamma = 478$ keV). The background was removed using a straight line between the average counting number/channel on both sides of the peak.

Figure 3 shows two exponential decay curves of the ^{7}Be radioactivities for samples of ^{7}Be@C_{70} at $T = 5$ K and ^{7}Be in Be metal at $T = 293$ K plotted against time (d). To compare the decay curves in Fig. 3, the data for the ^{7}Be@C_{70} were normalized to those for ^{7}Be in Be metal at Time = 0 (though the cps in both samples was approximately the same). Thus, the two decay curves can be compared under an exactly equal degree in the cps as vertical axis in Fig. 3. The red circle and blue crosses represent the radioactivities of the cps for the samples of ^{7}Be@C_{70} at $T = 5$ K and ^{7}Be in Be metal at $T = 293$ K. This difference in $T_{1/2}$ is sufficiently large and visually discernible, even when the data are shown on the extended scale of the panel on the right in Fig. 3.

The decay constants for the two samples were obtained by fitting a logarithmic function of the measured data points using the MINUIT program. The statistical errors associated with each data point were considered in this program. Here, the statistical errors in each red circle and the blue cross points were significantly small for dominant uncertainty. The uncertainty of our measurement corresponds to the uncertainty of the slope of the straight line fitted to the logarithm of the cps of the decay spectrum. The reduced χ-square values of the exponential fits are between 0.90 and 1.12; these values express the best fit for the precision. Uncertainty due to the dead time was estimated to be less than 0.04%, and the systematic error in the measurements was estimated to be less than half of the statistical error quoted above [26,27].

The measurements were performed twice for each sample at room ($T = 293$ K) and He ($T = 5$ K) temperatures for ^{7}Be@C_{70} using the sample of ^{7}Be in Be metal at $T = 293$ K and $T = 5$ K temperatures, respectively. The results are summarized in Fig. 4 (as the mean values) along with data points from previous studies for the ^{7}Be@C_{60} as shown by the full circle (black) and the open circle [26,27]. In the figure, the full circles (red and green) indicate the $T_{1/2}$ obtained for the ^{7}Be@C_{70} samples ($T = 293$ K and $T = 5$ K, respectively) and the crosses and square (blue) represent that for the ^{7}Be in Be metal ($T = 293$ K and $T = 5$ K), respectively, in Fig. 4.

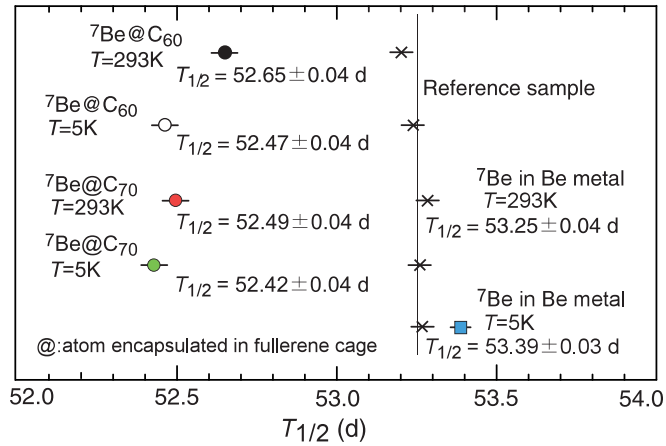

FIG. 4. $T_{1/2}$ measured in this period are plotted as closed colored circles (red for ^{7}Be@C_{70} at $T = 293$ K and green at $T = 5$ K). The measurement was performed twice for each sample, at room ($T = 293$ K) and He ($T = 5$ K) temperatures, for both ^{7}Be@C_{60} and ^{7}Be@C_{70} using the ^{7}Be sample in Be metal at $T = 293$ K. The crosses represent the $T_{1/2}$ used as the reference samples of ^{7}Be in Be metal at room ($T = 293$ K). The square (blue) represents the $T_{1/2}$ of ^{7}Be in Be metal at He temperature ($T = 5$ K) with the reference samples of ^{7}Be in Be metal at $T = 293$ K. All symbols show the mean values.

In this study, the average $T_{1/2}$ for the samples of ^{7}Be@C_{70} at $T = 293$ K and $T = 5$ K were $T_{1/2} = 52.49 \pm 0.04$ d and 52.42 ± 0.04 d, respectively. Furthermore, we obtained the average $T_{1/2}$ of ^{7}Be for the reference samples inside Be metal as $T_{1/2} = 53.25 \pm 0.04$ d (at $T = 293$ K) and $T_{1/2} = 53.39 \pm 0.03$ d (at $T = 5$ K). The $T_{1/2}$ obtained for ^{7}Be in ^{7}Be@C_{70}, $T_{1/2} = 52.42 \pm 0.04$ d ($T = 5$ K), was approximately 1.6% (1.8%) smaller than that for the ^{7}Be in the Be metal sample at $T = 293$ K (5 K), where the percentage difference is defined by $100 \times [(\lambda(\text{Be metal})\text{-}\lambda(C_{70}))/\lambda(\text{Be metal})]$. (Here, the relation between the $T_{1/2}$ and λ is presented above.) The $T_{1/2}$ measured for ^{7}Be@C_{60} at $T = 293$ K and 5 K were $T_{1/2} = 52.65 \pm 0.04$ d and 52.47 ± 0.04 d, respectively, and approximately 1.1% and 1.5% smaller than those for the ^{7}Be in the Be metal sample ($T = 293$ K). However, for ^{7}Be@C_{70} at $T = 293$ and 5 K, $T_{1/2} = 52.49 \pm 0.04$ d and 52.42 ± 0.04 d, respectively. In this study, the difference in the $T_{1/2}$ for ^{7}Be@C_{70} at $T = 293$ K and $T = 5$ K were considerably smaller than those for ^{7}Be@C_{60}, as shown in Fig. 4.

The relative differences could be strongly related to the potential configuration when the ^{7}Be remains inside the C_{60} and/or C_{70} cages, called the size effect between C_{60} and C_{70}. Furthermore, in terms of the differences for the same cages, C_{60} and/or C_{70}, at $T = 293$ K (and $T = 5$ K), inside these C_{60} and C_{70} cages, the Be atoms undergo a dynamical ratchet and/or tumbling motion [33–37], which may affect the contact electron density [$\rho(0)$] at the ^{7}Be nucleus. Several factors may contribute to creating this unique environment, for example, several π electrons of C_{70} and the special dynamic conditions of the electrons inside the C_{70} cage.

As the EC-decay rate is proportional to the electron density [$\rho(0)$] at the Be nucleus, we performed first-principles calculations using DMol^3 [38,39], wherein the numerical localized

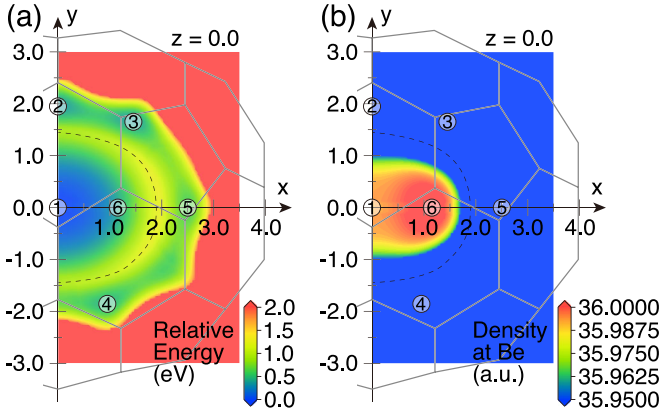

FIG. 5. Contour maps of (a) the relative total energy ΔE and (b) the electron density at the Be nucleus $\rho(0)$ on the XY plane inside C_{70}.

orbitals were used. The double-numeric quality basis set with polarization functions (DNP) and the BLYP exchange-correlation functional were used as in our previous studies [27,28,41]. The calculations were performed at 8942 points on 0.05 Å fine grids in the XY and YZ planes, where the X and Y coordinates are the longer and shorter molecular axes going through the center of a six-membered ring at the equator, respectively. The Z coordinate is perpendicular to these axes. The most stable point was the center (0,0,0) of C_{70} as expected from a previous calculation [30]. The relative total energy ΔE and electron density [$\rho(0)$] are shown on the XY plane in Fig. 5. The spin magnetic moment M was 0 μ_B (2 μ_B) inside (outside) the dashed line. The values of ΔE, M, and $\rho(0)$ at certain typical points (numbered on Fig. 5) are listed in Table I. The metastable point was located at (0, 1.95 Å, 0) (No. 2) just below the center of a six-membered ring on the equator perpendicular to the longer molecular axis. However, the energy difference from the C_{70} center was 0.360 eV, which is greater than 0.068 eV for C_{60} [27,28]. Moreover, as listed in Table I, the electron density at the Be nucleus, when it is located at the metastable position close to the cage surface, is 1.8% smaller than that at the center of C_{70} and C_{60}. This explains our experimental evidence that the $T_{1/2}$ does not change significantly at the liquid helium and room temperatures. This characteristic is evidently different from Be@C_{60}, which showed significant temperature dependence [27,28]. The electron density [$\rho(0)$] was the highest at (1.15 Å, 0, 0) (No. 6) and second highest at (0,0,0), which was slightly lower than that of Be@C_{60} [27,28], although the difference was very small. This is consistent with the experimental evidence that the $T_{1/2}$ of ^{7}Be@C_{70} is close to that of ^{7}Be@C_{60} at $T = 5$ K when ^{7}Be is frozen at the center of C_{60}. In other explanation, first-principles calculations showed that ^{7}Be can enter the metastable position of C_{60} at room temperature but cannot enter the metastable position of C_{70} owing to the difference in potential configuration. Therefore, the results for the $T_{1/2}$ of ^{7}Be@C_{70} at $T = 293$ K and 5 K agree within the uncertainties, while that for C_{60} at $T = 293$ K and 5 K appears larger.

TABLE I. Position [No. in Fig. 5 and X, Y coordinates on the XY ($Z = 0$) plane], relative total energy ΔE (eV), magnetic moment M (μ_B), and the electron density at the Be nucleus, $\rho(0)$ (e^-/a_B^3).

No.	X (Å)	Y (Å)	ΔE (eV)	M (μ_B)	$\rho(0)$ ($e^-/a_B{}^3$)
1	0.00	0.00	0.000	0	35.990
2	0.00	1.95	0.360	2	35.330
3	1.45	1.65	0.377	2	35.314
4	0.95	−1.85	0.465	2	35.325
5	2.50	0.00	0.613	2	35.336
6	1.15	0.00	0.393	0	36.007
center of C_{60}			—	0	36.016
under 5-mem. ring of C_{60}			0.068	2	35.287

Recently, Bibikov *et al.* reported the ΔE curves along the X, Y, and Z axes using MP2 calculations [30]. Despite the lack of metastable position inside C_{70} in the curves, their result can explain our experimental conclusion that the $T_{1/2}$ does not change significantly at 5 K and 293 K. Moreover, their result indicates that Be@C_{60} has a slightly higher $\rho(0)$ than Be@C_{70}, which concurs with our BLYP result.

Furthermore, it is interesting to note that electron-phonon couplings are larger in C_{60} than in C_{70} [42,43], and they may play a role in determining the EC-decay rate. This question remains to be understood both theoretically and experimentally.

In this study, the $T_{1/2}$ (EC-decay rate of ^{7}Be) of the samples of ^{7}Be@C_{60} and ^{7}Be@C_{70}, and the ^{7}Be in Be metal, were experimentally compared. Here, the 2s electrons of ^{7}Be in C_{70} can be restricted to the Be atom at $T = 5$ K (even at $T =$ 293 K including dynamical and/or static motion) [27,28]. For ^{7}Be@C_{70}, although the Be atom does not visit the metastable positions (Nos. 2–6) owing to their high ΔE, there is no metastable position inside C_{70}. However, we found that the electron density [$\rho(0)$] was the highest at 1.15 Å in the longer axis [second highest at center as shown in Fig. 5(b)], which is slightly lower than that of Be@C_{60} case [27,28]. These results can also explain our experimental conclusions regarding the $T_{1/2}$ minimal change at 5 and 293 K, where, the dynamical and/or static motion are not conceivably important because of the size of the C_{70} cage. Furthermore, these values for ^{7}Be@C_{70} at $T = 5$ K are approximately 1.6%(1.8%) smaller than those for ^{7}Be in Be metal at $T = 293$ K ($T = 5$ K). The $T_{1/2}$ of ^{7}Be in Be metal was $T_{1/2} = 53.25 \pm 0.04$ d at $T = 293$ K and $T_{1/2} = 53.39 \pm 0.03$ d at $T = 5$ K. We are still considering the difference between at $T = 293$ and 5 K in Be metal, which is at most around 0.26%, but is clearly different [44].

The magnitude of the average charge transfer from 2s electrons of the ^{7}Be atom, e.g., the L capture, can play an important role in such a large variation in the EC-decay rate of ^{7}Be [28,45,46]. The mechanism indicates that increasing the electron density [$\rho(0)$] at the nucleus increases the EC-decay rate (shortens the $T_{1/2}$). Although Be is an alkaline earth metal, which is usually used (preferred) in the Be^{2+} state, the charge state of Be atom inside C_{70} (and/or C_{60}) can be approximately near the neutrality form. The electronic shield effect is substantially influenced by the potential configuration of

the continuous neutral charge state inside C_{70} (and/or C_{60}). In contrast, the reported values for $T_{1/2}$ are approximately 53.12 and/or 53.22 d (see *Table of Isotopes* [47], NUBASE2020 [48]), owing to the valence number of near Be^{2+} caused by chemical bond and/or metallic (crystallized) state in realistic materials.

Finally, we found that the $T_{1/2}$ of ^{7}Be inside C_{70} was considerably smaller than that reported in any previous study for different environments, material, and/or pressure, implying that the ^{7}Be atoms are within a unique environment. Even an extreme pressure and/or a continuous change in the charge state under specific environments (involving further complicated experimental processes) may change the EC-decay rate by a certain magnitude. However, our limited observed effects could still significantly raise the magnitude of parameters achievable in laboratories. Furthermore, the results of this study, the physical and/or chemical properties of the radionuclide-encapsulating fullerenes, are expected to promote research in related fields.

In conclusion, this study measured the $T_{1/2}$ of ^{7}Be alternately using a reference method, one for ^{7}Be encapsulated in C_{70} and the other for ^{7}Be incorporated in Be metal. An HPGe detector accepting a standard-time radio signal was used to perform the measurements. We found that the $T_{1/2}$ of ^{7}Be inside C_{70} were $T_{1/2} = 52.49 \pm 0.04$ d and 52.42 ± 0.04 d at $T = 293$ and 5 K, respectively. Furthermore, the $T_{1/2}$ of ^{7}Be in Be metal was $T_{1/2} = 53.25 \pm 0.04$ d at $T = 293$ K (and $T_{1/2} = 53.39 \pm 0.03$ d at $T = 5$ K). This difference of 1.4% (1.8%) in the EC-decay rate between the host of C_{70} and Be metal at $T = 293$ K ($T = 5$ K) indicates different electronic wave functions [the electron density ($\rho(0)$)] inside each material. The ^{7}Be EC-decay rate inside C_{70} exhibited a unique environmental effect. We performed first-principles calculations using DMol^3, employing numerical localized orbitals. As no metastable site was visited inside C_{70}, their results can explain our observed minimal change in $T_{1/2}$ at $T = 5$ K and 293 K for ^{7}Be@C_{70}, which is clearly different for ^{7}Be@C_{60}. The change in $T_{1/2}$ in ^{7}Be was related to the potential configuration and environment inside fullerene cages. The motion of ^{7}Be inside the cages was restricted according to the temperature, which has not been observed in previous studies.

This work was supported by JSPS KAKENHI Grants No. 16K15579, No. 18H04150, No. 19K22596 for T.O. and No. 21H01877 for K.O. Moreover, the authors are grateful to the staff at the division of accelerators of the Laboratory of Nuclear Science and the Cyclotron Radio-Isotope Center, Tohoku University, and the Institute for Integrated Radiation and Nuclear Science, Kyoto University.

[1] E. Segrè, Phys. Rev. **71**, 274 (1947); E. Segrè and C. E. Wiegand, *ibid.* **75**, 39 (1949).
[2] R. Daudel, Rev. Sci. **85**, 162 (1947).
[3] R. F. Leininger, E. Segrè, and C. Wiegand, Phys. Rev. **76**, 897 (1949).
[4] J. J. Kraushaar, Elizabeth D. Wilson, and Kenneth T. Bainbridge, Phys. Rev. **90**, 610 (1953).
[5] G. T. Emery, Annu. Rev. Nucl. Sci. **22**, 165 (1972).
[6] H. W. Johlige, D. C. Aumann, and H. J. Born, Phys. Rev. C **2**, 1616 (1970).
[7] C. A. Huh, Earth Planet. Sci. Lett. **171**, 325 (1999).
[8] J. A. Tossell, Earth Planet. Sci. Lett. **195**, 131 (2002).
[9] F. Lagoutine, J. Legrand, and C. Bac, Int. J. appl. Radiat. Isotopes **26**, 131 (1975).
[10] W. K. Hensley, W. A. Bassett, and J. R. Huizenga, Science **181**, 1164 (1973).
[11] L. G. Liu and C. A. Huh, Earth Planet. Sci. Lett. **180**, 163 (2000).
[12] A. Ray, A. K. Sikdar, P. Das, S. Pathak, and J. Datta, Phys. Rev. C **101**, 035801 (2020).
[13] M. Jaeger, S. Wilmes, V. Kölle, G. Staudt, and P. Mohr, Phys. Rev. C **54**, 423 (1996).
[14] A Ray, P. Das, S. K. Saha, S. K. Das, B. Sethi, A. Mookerjee, C. Basu Chaudhuri, and G. Pari, Phys. Lett. B **455**, 69 (1999).
[15] E. B. Norman, G. A. Rech, E. Browne, R. M. Larimer, M. R. Dragowsky, Y. D. Chan, M. C. P. Isaac, R. J. McDonald, and A. R. Smith, Phys. Lett. B **519**, 15 (2001).
[16] A. Ray, P. Das, S. K. Saha, and S. K. Das, Phys. Lett. B **531**, 187 (2002).
[17] L. Zhi-Yi, C. B. Li, S. G. Wang, J. Zhou, Q. Y. Meng, Q. Y. Lu, and S. H. Zhou, Chinese Phys. Lett. **20**, 829 (2003).
[18] B. N. Limata, Zs. Fülöp D. Schürmann, N. De Cesare, A. DÓnofrio, A. Esposito, L. Gialanella, Gy. Gyürky, G. Imbriani, F. Raiola, V. Roca1, D. Rogalla, C. Rolfs, M. Romano, E. Somorjai, F. Strieder, and F. Terras, Eur. Phys. J. A **27**, 193 (2006).
[19] Y. Nir-El, G. Haquin, Z. Yungreiss, M. Hass, G. Goldring, S. K. Chamoli, B. S. Nara Singh, S. Lakshmi, U. Köster, N. Champault, A. Dorsival, G. Georgiev, V. N. Fedoseyev, B. A. Marsh, D. Schumann, G. Heidenreich, and S. Teichmann, Phys. Rev. C **75**, 012801(R) (2007).
[20] V. Kumar, M. Hass, Y. Nir-El, G. Haquin, and Z. Yungreiss, Phys. Rev. C **77**, 051304(R) (2008).
[21] T. Ohtsuki, K. Masumoto, K. Sueki, K. Kobayashi, and K. Kikuchi, J. Am. Chem. Soc. **117**, 12869 (1995).
[22] T. Ohtsuki, K. Masumoto, K. Ohno, Y. Maruyama, Y. Kawazoe, K. Sueki, and K. Kikuchi, Phys. Rev. Lett. **77**, 3522 (1996).
[23] T. Ohtsuki, K. Ohno, K. Shiga, Y. Kawazoe, Y. Maruyama, and K. Masumoto, Phys. Rev. Lett. **81**, 967 (1998).
[24] T. Ohtsuki, K. Ohno, K. Shiga, Y. Kawazoe, Y. Maruyama, and K. Masumoto, Phys. Rev. B **60**, 1531 (1999).
[25] T. Ohtsuki, A. Manjanath, K. Ohno, M. Inagaki, S. Sekimoto, and Y. Kawazoe, RSC Adv. **11**, 19666 (2021).
[26] T. Ohtsuki, H. Yuki, M. Muto, J. Kasagi, and K. Ohno, Phys. Rev. Lett. **93**, 112501 (2004).
[27] T. Ohtsuki, K. Ohno, T. Morisato, T. Mitsugashira, K. Hirose, H. Yuki, and J. Kasagi, Phys. Rev. Lett. **98**, 252501 (2007).

[28] T. Morisato, K. Ohno, T. Ohtsuki, K. Hirose, M. Sluiter, and Y. Kawazoe, Phys. Rev. B **78**, 125416 (2008).
[29] E. V. Tkalya, A. V. Bibikov, and I. V. Bodrenko, Phys. Rev. C **81**, 024610 (2010).
[30] A. V. Bibikov, A. V. Nikolaev, and E. V. Tkalya, Phys. Rev. C **100**, 064603 (2019).
[31] F. Gholamian, M. M. Firoozabadi, and H. Raissi, Phys. Rev. C **102**, 014606 (2020).
[32] A. Yoshida, M. Abe, and M. Hada, J. Phys. Chem. A **125**, 29, 6356 (2021).
[33] K. Ohno, Y. Maruyama, K. Esfarjani, Y. Kawazoe, N. Sato, R. Hatakeyama, T. Hirata, and M. Niwano, Phys. Rev. Lett. **76**, 3590 (1996).
[34] W. Sato, K. Sueki, Y. Achiba, H. Nakahara, Y. Ohkubo, and K. Asai, Phys. Rev. B **63**, 024405 (2000).
[35] B. W. Smith, D. E. Luzzi, and Y. Achiba, Chem. Phys. Lett. **331**, 137 (2000).
[36] R. Jorn, J. Zhao, H. Petek, and T. Seideman, ACS Nano **5**, 7858 (2011).
[37] S. Aoyagi, K. Miwa, H. Ueno, H. Okada, Y. Matsuo, and K. Kokubo, R. Soc. Open Sci. **5**, 180337 (2018).
[38] B. Delley, J. Chem. Phys. **92**, 508 (1990).
[39] B. Delley, J. Chem. Phys. **113**, 7756 (2000).
[40] T. Ohtsuki, K. Masumoto, K. Sueki, K. Kikuchi, K. Ohno, Y. Maruyama, and Y. Kawazoe, AIP Conf. Proc. **416**, 261 (1997).
[41] S. Ono, R. Kuwahara, T. Morisato, and K. Ohno, Chem. Phys. Lett. **561–562**, 137 (2013).
[42] D. Provasi, N. Breda, R. A. Broglia, G. Colo, H. E. Roman, and G. Onida, Phys. Rev. B **61**, 7775 (2000).
[43] N. Breda, R. A. Broglia, G. Colo, H. E. Roman, F. Alasia, G. Onida, V. Ponomarev, and E. Vigezzi, Chem. Phys. Lett. **286**, 350 (1998).
[44] R. Kuwahara, K. Ohno, and T. Ohtsuki (unpublished).
[45] P. A. Voytas, C. Ternovan, M. Galeazzi, D. McCammon, J. J. Kolata, P. Santi, D. Peterson, V. Guimarães, F. D. Becchetti, M. Y. Lee, T. W. ODonnell, D. A. Roberts, and S. Shaheen, Phys. Rev. Lett. **88**, 012501 (2001).
[46] A. Ray, P. Das, S. K. Saha, S. K. Das, and A. Mookerjee, Phys. Rev. C **66**, 012501(R) (2002).
[47] R. B. Firestone, C. M. Baglin, and S. Y. Frank Chu (eds.), *Table of Isotopes*, 8th ed. (John Wiley & Sons, New York, 1999).
[48] NUBASE Evaluation of nuclear properties, NUBASE2020, IAEA-Nuclear Data Section, https://www-nds.iaea.org/relnsd/vcharthtml/VChartHTML.html.